Closed-loop measurements in an atom-interferometer gyroscope with compensation for velocity-dependent phase dispersion

Tomoya Sato,[1] Naoki Nishimura,[2] Naoki Kaku,[2] Sotatsu Otabe,[1,†] Takuya Kawasaki,[1,†] Toshiyuki Hosoya,[3] and Mikio Kozuma[1,2,*]

[1] *Institute of Integrated Research, Institute of Science Tokyo, 4259 Nagatsuta-cho, Midori-ku, Yokohama, Kanagawa 226-8501, Japan*

[2] *Department of Physics, Institute of Science Tokyo, 2-12-1 Ookayama, Meguro-ku, Tokyo 152-8550, Japan*

[3] *Product Development Center, Japan Aviation Electronics Industry, Ltd., 3-1-1, Musashino, Akishima-shi, Tokyo 196-8555, Japan*

(Received 8 July 2024; revised 15 January 2025; accepted 12 March 2025; published 1 April 2025)

Atom-interferometer-based gyroscopes are expected to have a wide range of applications due to their high sensitivity; however, their dynamic range is limited by dephasing from the velocity-dependent Sagnac phase shift and the longitudinal velocity distribution of the atoms, restricting measurements of large angular velocities. In this study, we present a method for restoring the contrast deterioration in angular velocity measurements with interferometer gyroscopes using atomic beams. We show that by introducing a pseudorotation effect with appropriate two-photon detunings for Raman light in the interferometer, it is possible to effectively cancel the Sagnac phase shift for all atoms in the velocity distribution of the beam. Consequently, the contrast is unaffected by the rotation. Furthermore, we apply this method to an interferometer gyroscope with counterpropagating atomic beams sharing the same Raman light. It is found that the angular velocity of the system can be estimated through the detuning point where the phase difference between the two interferometers is zero. This approach ensures that the scale factor of the atom interferometer gyroscope is independent of the change in the longitudinal velocity distribution of the atomic beam. We demonstrate our technique using an interferometer gyroscope with thermal atomic beams of rubidium-87, achieving a measurement of angular velocity of 1.0 °/s even with an acceleration of 0.68 m/s^2 on a three-axis rotation table. This simple and robust dispersion-compensation method with Raman-light detuning will benefit dynamic angular velocity measurements in field applications such as the inertial navigation of vehicles.

DOI: 10.1103/PhysRevApplied.23.044001

I. INTRODUCTION

In the three decades following its inception [1,2], light-pulse atom interferometry has been actively researched as a sensing tool across many fields for measuring acceleration [3,4], angular velocity [5–9], gravity [10–12], gravity gradients [13,14], fundamental constants [15,16], gravitational waves [17–20], and dark matter and dark forces [20,21]. In recent years, the performance of atom-interferometry-based inertial sensors has reached the level of field applications [22–26] due to their improved sensitivity and accuracy. Among various applications, these sensors are notably expected to be employed in inertial navigation [27]. Inertial navigation is a method for estimating the position of an object without relying on external references such as the Global Positioning System, and it requires highly accurate angular velocity and acceleration sensors. The accuracy of conventional inertial sensors, such as fiber-optic gyroscopes (FOGs), has significantly improved in recent years [28–30]; however, the expected high sensitivity that atom interferometry would bring is essential for highly accurate inertial navigation [31–33].

For inertial navigation, the sensors should possess a high dynamic range of measurement, and this presents a primary research obstacle in employing atom interferometry in inertial sensors. In atom interferometry, angular velocity and acceleration cause shifts in the interference phase, and this is known as the "Sagnac effect" for angular velocity [34–36]. The magnitude of these phase shifts depends on the velocity of the atoms. Due to the longitudinal velocity distribution of atoms, the phase shift due to the angular velocity or acceleration will also have a dispersion, resulting in signal loss when the average phase

*Contact author: kozuma@qnav.iir.isct.ac.jp

†Present address: Department of Physics, University of Tokyo, 7-3-1 Hongo, Bunkyo-ku, Tokyo 113-0033, Japan.

shift is observed. This effect becomes more intense as the width of the velocity distribution increases relative to the average speed of the atoms. One of the most successful methods for extending the dynamic range is to compress the longitudinal velocity distribution of an atomic beam using laser-cooling techniques. Kwolek *et al.* [37] produced an atomic beam with a narrow velocity distribution by extracting laser-cooled and trapped atoms as a continuous beam. They irradiated these atoms with light detuned to the Doppler shift corresponding to the desired longitudinal velocity. d'Armagnac de Castanet *et al.* [38] developed an alternative method for inertial sensing using a cold-atom interferometer. They extended the dynamic measurement range by mechanically changing the direction of the laser light within the interferometer to counteract the effects of the applied acceleration and angular velocity measured using classical sensors. Although these methods are helpful, building them into a compact system is difficult because they require additional optics and light sources for laser cooling, as well as additional mechanical structures. Moreover, these additional components may introduce instability. Achieving high accuracy in measuring and controlling the velocity of atoms is also challenging. Therefore, instability in the longitudinal velocity affects the stability of the angular velocity measurements, particularly because the scale factor depends on the longitudinal velocity.

In this study, we demonstrate a closed-loop method for phase-dispersion compensation that can enhance the dynamic range of inertial sensors using a spatial-domain interferometer. Importantly, this enhancement is achieved without adding any new elements. This is accomplished simply by adjusting the two-photon detuning of the Raman light that composes the interferometer. Our method involves phase compensation that is dependent on the time of flight of the atoms between light beams, i.e., the longitudinal velocity of the atoms. The concept of velocity-dependent phase-dispersion compensation was proposed and demonstrated through the precise measurement of the electric polarizability of a sodium atom [39]. The phase shift due to the interaction between the atom and the electric field was compensated using a phase shifter, which creates electric field gradients, introducing a phase shift that is inversely proportional to the velocity of the atoms. Another type of phase shifter using optical prism pairs has been proposed for use in electrical polarizability measurements [40]. Gustavson *et al.* [5] successfully measured the Earth's rotation rate using a phase shifter that uses Raman light beams to construct an atom interferometer; by temporally sweeping the two-photon detuning of Raman light beams and performing theoretical fitting on the resulting interferometer output, they determined the value that effectively canceled the Doppler shift induced by the Earth's rotation.

In this work, we experimentally demonstrated the real-time measurement of angular velocity using a closed-loop technique. We present a detailed calculation of the velocity-dependent phase-dispersion compensation for continuously measuring the angular velocity of a system using dual-beam atom interferometers. In addition, we demonstrated our method using an atom interferometer gyroscope (AIG) with dual thermal atomic beams mounted on a three-axis rotation table. The experimentally measured scale factor remained unchanged even when acceleration was applied, causing the velocity of the atomic beam to vary during its time of flight. Furthermore, the dynamic range of angular velocity measurements was successfully extended through the use of a closed-loop technique. Note that a similar technique, using single-photon detuning rather than the two-photon detuning of Raman light applied in our method [41], has been proposed to eliminate the effect of the gravitational gradient in the universality of free-fall experiments using atom interferometers [42,43].

II. ROTATION COMPENSATION WITH THE TWO-PHOTON DETUNING OF RAMAN LIGHT BEAMS

Let us consider a $\pi/2$–π–$\pi/2$ Mach-Zehnder-type atom interferometer using Raman transitions. Here, we provide an overview of the Raman transitions and interferometers (details can be found in Refs. [5,44]). Figure 1 shows a space-time diagram of the single-beam interferometer. An atom in the ground state $|1\rangle$, with an excited state $|2\rangle$ whose energy is $\hbar\omega_0$ higher than $|1\rangle$ (where $\hbar$ is the reduced Planck constant), travels at a longitudinal velocity v. When this atom is irradiated with a pair of counter-propagating laser beams, a two-photon Raman transition between $|1\rangle$ and $|2\rangle$ occurs. Atoms transitioning to the $|2\rangle$ state through the Raman transition receive recoil momentum $\hbar(\boldsymbol{k_1} - \boldsymbol{k_2})$ from the beams, where $\boldsymbol{k_1}$ and $\boldsymbol{k_2}$ are the wave vectors of the pair of laser beams. This causes the atoms in the two states to travel different paths. The wavelengths of the beams are sufficiently detuned by Δ from the excited state $|e\rangle$ to avoid an actual excitation, and their frequency difference is tuned to $\omega_0 + \omega_r$, where $\omega_r = \hbar(k_1 + k_1)^2/(2m)$ is a recoil frequency and m is the mass of the atom. An interferometer can be constructed by setting the two-photon Rabi frequency determined by the intensity of the Raman light such that the first, second, and final Raman beams induce 50%, 100%, and 50% transitions, respectively. The population of atoms in the $|2\rangle$ state after passing through the interferometer can be expressed

as follows:

$$P_2(\boldsymbol{\Omega}, \boldsymbol{a}) = \frac{1}{2}\left\{1 - \cos\left[\boldsymbol{k}_{\text{eff}} \cdot (2\boldsymbol{\Omega} \times \boldsymbol{v} + \boldsymbol{a})\left(\frac{L}{v}\right)^2 + \phi_{\text{laser}}\right]\right\}, \tag{1}$$

where $\boldsymbol{k}_{\text{eff}} = \boldsymbol{k_1} - \boldsymbol{k_2}$ is an effective k vector for the Raman transition, $\boldsymbol{\Omega}$ and $\boldsymbol{a}$ are the angular velocity and acceleration vectors of the system, respectively, $\boldsymbol{v}$ is the velocity vector of the atom, L is the spatial separation between Raman beams, and ϕ_{laser} is an arbitrary laser phase. This laser phase can be expressed using the phases of each Raman beam ϕ_i $(i = 1, 2, 3)$ as $\phi_{\text{laser}} = (\phi_1 - 2\phi_2 + \phi_3)$. Here, we assume that the phase outputs of the interferometers are measured simultaneously using counterpropagating atomic beams that share Raman light beams (AIG configuration). The velocity vector of the left-oriented atomic beam, $\boldsymbol{v}_{\text{L}}$, exhibits an opposite sign to that of the right-oriented beam $\boldsymbol{v}_{\text{R}} = -\boldsymbol{v}_{\text{L}} = \boldsymbol{v}$. Due to the orientation dependence of the velocity vector in the phase term of Eq. (1), the rotation term is sign-reversed for both atomic beams, whereas the acceleration term and arbitrary laser phase remain unchanged. Thus, by considering the phase difference between two interferometers, we can obtain the phase shift due only to the rotation, which can be expressed as $4\boldsymbol{k}_{\text{eff}} \cdot \boldsymbol{\Omega} \times \boldsymbol{v}(L/v)^2$.

With the longitudinal velocity distribution of the atoms $f(v)$, Eq. (1) can be modified as follows:

$$P_2(\boldsymbol{\Omega}, \boldsymbol{a}) = \frac{1}{2}\int_0^\infty f(v) \times \left\{1 - \cos\left[\boldsymbol{k}_{\text{eff}} \cdot (2\boldsymbol{\Omega} \times \boldsymbol{v} + \boldsymbol{a})\left(\frac{L}{v}\right)^2 + \phi_{\text{laser}}\right]\right\} dv. \tag{2}$$

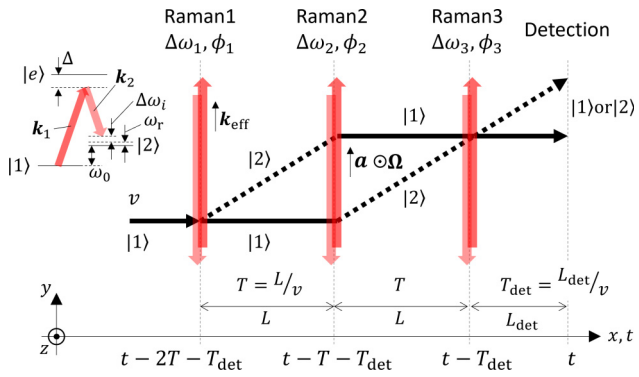

FIG. 1. Space-time diagram of a $\pi/2$–π–$\pi/2$ Mach-Zehnder-type atom interferometer using Raman transitions.

Due to the finite velocity distribution of the atoms used for the measurement, the phase of the rotating interferometer will have dispersion. At high angular velocity, the interference contrast deteriorates, limiting the dynamic range of the AIG. For example, with the atomic beam of rubidium (Rb)-87 from the thermal atomic beam source at 100 °C, the contrast decreases to $1/e$ at an angular velocity of 0.6 °/s with the Raman light separation set at $L = 70$ mm.

To restore the decrease in contrast with rotation, we introduce a velocity-dependent compensation for the Sagnac phase shift using two-photon detuning of the Raman light. The time-dependent phases of the Raman lasers $\phi_{t,i=1,2,3}(t)$ can be written as follows:

$$\phi_{t,i}(t) = (\omega_0 + \Delta\omega_i)t + \phi_i, \tag{3}$$

where $\Delta\omega_i$ is the two-photon detuning from the resonance of the Raman transition in units of angular frequency (see Fig. 1). As shown in the lower part of Fig. 1, the time at which an atom interacts with each Raman beam depends on its longitudinal velocity. This implies that atoms receive different phases from the Raman light depending on their velocity because the phase of the Raman light is swept linearly according to the $\Delta\omega_i t$ term in Eq. (3). The phase output of the right-oriented atom interferometer is expressed as follows:

$$\begin{aligned}\Phi_R(t, \Omega, a) &= 2k_{\text{eff}}\Omega\frac{L^2}{v} + k_{\text{eff}}a\frac{L^2}{v^2} \\ &\quad + (\omega_0 + \Delta\omega_1)(t - 2T - T_{\text{det}}) + \phi_1 \\ &\quad - 2\left[(\omega_0 + \Delta\omega_2)(t - T - T_{\text{det}}) + \phi_2\right] \\ &\quad + (\omega_0 + \Delta\omega_3)(t - T_{\text{det}}) + \phi_3 \\ &= 2k_{\text{eff}}\Omega\frac{L^2}{v} + k_{\text{eff}}a\frac{L^2}{v^2} \\ &\quad - \left[(2L + L_{\text{det}})\Delta\omega_1\right. \\ &\qquad \left. - 2(L + L_{\text{det}})\Delta\omega_2 + L_{\text{det}}\Delta\omega_3\right]\frac{1}{v} \\ &\quad + (\Delta\omega_1 - 2\Delta\omega_2 + \Delta\omega_3)t + \phi_{\text{laser}},\end{aligned} \tag{4a}$$

where $T = L/v$ is the time of flight between Raman light beams with separation L, while $T_{\text{det}} = L_{\text{det}}/v$ is the time of flight between the final Raman beam and the probe beam with separation L_{det} (this derivation for a single interferometer can also be found in Ref. [45]). For simplicity, we assume that $\boldsymbol{v}$ is aligned along the x axis, $\boldsymbol{k}_{\text{eff}}$ and $\boldsymbol{a}$ are aligned along the y axis, and $\boldsymbol{\Omega}$ is aligned along the z axis, i.e., $\boldsymbol{v} = (v, 0, 0)$, $\boldsymbol{k}_{\text{eff}} = (0, k_{\text{eff}}, 0)$, $\boldsymbol{a} = (0, a, 0)$, and $\boldsymbol{\Omega} = (0, 0, \Omega)$. Similarly, the phase output for the left-oriented atom interferometer (not shown in Fig. 1) can be

written as follows:

$$\Phi_L(t,\Omega,a) = -2k_{\text{eff}}\Omega\frac{L^2}{v} + k_{\text{eff}}a\frac{L^2}{v^2} - [L_{\text{det}}\Delta\omega_1 - 2(L+L_{\text{det}})\Delta\omega_2 + (2L+L_{\text{det}})\Delta\omega_3]\frac{1}{v} + (\Delta\omega_1 - 2\Delta\omega_2 + \Delta\omega_3)t + \phi_{\text{laser}}. \quad (4b)$$

We assume that L_{det} is the same for both atomic beams. The first term represents the velocity-dependent Sagnac phase, which causes the dephasing of the interference signal. Since the third term is proportional to $1/v$, the phase shift resulting from the Sagnac effect can be nullified by appropriately setting the sign and value for the two-photon detunings. When we set the two-photon detunings as $\Delta\omega_1 = k_{\text{eff}}\Omega L$, $\Delta\omega_2 = 0$, and $\Delta\omega_3 = -k_{\text{eff}}\Omega L$, the relative phase between the two interferometers becomes zero for an atom at any given longitudinal velocity:

$$\Delta\Phi(\Omega) = \Phi_R(t,\Omega,a) - \Phi_L(t,\Omega,a) = 4k_{\text{eff}}\Omega\frac{L^2}{v} - 2(\Delta\omega_1 - \Delta\omega_3)\frac{L}{v} = 0. \quad (5)$$

This result shows that closed-loop measurements can be conducted by controlling the value of the detunings to maintain the condition of $\Delta\Phi = 0$. Such measurements have three advantages, which are as follows:

(1) The dynamic range of the rotation measurement using an atom interferometer can be extended compared to open-loop measurements. By using closed-loop measurements, the system can be treated as effectively stationary. As a result, the phase dispersion from the velocity-dependent phase shift caused by the rotation vanishes, thus preventing the dephasing. This is particularly beneficial for an AIG with a thermal atomic beam, since it is challenging to implement advanced techniques for suppressing the longitudinal velocity distribution, such as 3D cooling in a cold atomic beam [37].

(2) The angular velocity measurement of the system is independent of the longitudinal velocity of the atoms. Without the closed-loop operation, the angular velocity is directly derived from the Sagnac phase shift using the following equation:

$$\Omega = \frac{\Delta\Phi(\Omega)v}{4k_{\text{eff}}L^2}. \quad (6)$$

Precise determination and control of the mean and distribution of the atom velocities are challenging, particularly for thermal atomic beams. The limited stability of the velocity of the atoms causes errors in the estimation of angular velocities. With the closed-loop operation, the measured angular velocity no longer depends on the velocity of the atom:

$$\Omega = \frac{\Delta\omega_1}{k_{\text{eff}}L} = -\frac{\Delta\omega_3}{k_{\text{eff}}L}. \quad (7)$$

(3) The acceleration does not contribute to systematic error in the rotation measurement because the phase shift caused by the acceleration is the same for both interferometers in Eq. (5).

Regarding the advantage of point 3, it is important to note that the interference contrast diminishes as the acceleration increases; however, this contrast reduction can be partially compensated by setting the two-photon detuning of the second Raman beam to $\Delta\omega_2 = -k_{\text{eff}}aL^2/[2(L+L_{\text{det}})v]$ [see Eq. (4a)]. Due to the $1/v^2$ dependence of the phase shift caused by the acceleration, the compensation is partial and affected by the longitudinal velocity of the atoms. For example, with an atomic beam of ^{87}Rb from an oven at 100 °C and a Raman light separation of $L = 70$ mm, the contrast decreases to $1/e$ at an acceleration of 4 m/s^2 which can be improved to 1×10^1 m/s^2 with compensation. Since a nonzero $\Delta\omega_2$ works as a shared acceleration for dual interferometers, it does not introduce systematic error in the rotation measurement.

The theory of closed-loop measurement for a single-beam atom gyroscope was proposed by Joyet *et al.* [46]. Unlike their approach, our method, which uses dual atomic beams, offers advantages 2 and 3 mentioned above in the presence of acceleration.

III. EXPERIMENTAL DEMONSTRATION OF CLOSED-LOOP ROTATION COMPENSATION

We demonstrated our phase-dispersion compensation method using an AIG with thermal atomic beams of ^{87}Rb. Figure 2 shows a schematic of the experimental setup. We constructed a pair of atom interferometers with counter-propagating atomic beams that shared three Raman light beams. An atomic beam of Rb was extracted from the vapor source at approximately 100 °C through a glass capillary plate with a thickness and hole diameter of 0.5 mm and 4 μm, respectively. The initial state of the atoms was prepared in the $m_F = 0$ of $F = 1$ hyperfine ground state using two pumping laser beams tuned to the $F = 2$–$F' = 2$ and $F = 1$–$F' = 1$ transitions of ^{87}Rb. A $\pi/2$–π–$\pi/2$ Mach-Zehnder-type atom interferometer was constructed using three pairs of Raman light beams spatially separated by 70 mm. Each pair of Raman light beams was composed of two counterpropagating lasers, whose wavelengths are illustrated in Fig. 2. These beams induced the transition between the $F = 1$ and $F = 2$ hyperfine ground states through a Doppler-sensitive Raman transition. The Raman beams were detuned by $\Delta/2\pi = 1.5$ GHz from the $F' = 0$ state. The vertical and horizontal waists of each Raman

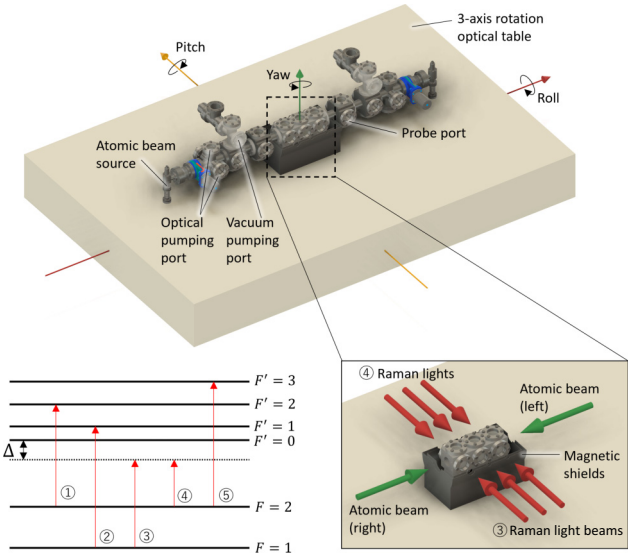

FIG. 2. Experimental setup for closed-loop measurements using AIG. The legends for one atomic interferometer apply similarly to the other interferometer. ① Hyperfine pumping light, ② Zeeman pumping light, ③ and ④ Raman beams, ⑤ probe light.

light were 18 mm and 190 μm, respectively. The powers of Raman beams 1, 2, and 3 were set at 30, 60, and 30 mW, respectively, to achieve the highest interference contrast. The relative phases of the three pairs of counterpropagating Raman light beams were measured using the optical beat detection technique, and the beams were phase locked to a single radio-frequency reference. According to the fourth terms in Eqs. (4a) and (4b), we can sweep the phase of the interferometer linearly by using nonzero two-photon detuning for the Raman light. This was achieved by inserting an acousto-optic modulator into one of the two beams comprising each Raman beam pair. For rotation compensation, the two-photon detunings of Raman beams 1 and 3 had equal absolute values with opposite signs. Moreover, these detunings were dynamically adjusted such that the difference between the phase outputs of the two interferometers was equal to the value observed when the rotation table was stationary. We employed $\Delta\omega_2/2\pi = 100$ Hz, resulting in modulation of the population in the $F = 2$ state sinusoidally at 200 Hz. Note that, for our experimental parameters, the value of $\Delta\omega_2/2\pi$ that degrades the contrast to $1/e$ is estimated to be 6×10^2 Hz, which is derived from Eqs. (2) and (4a) with $L_{\mathrm{det}} = 125$ mm. The interference phase can be deduced by irradiating a probe laser resonant with the $F = 2$–$F' = 3$ cyclic transition and performing a lock-in detection of the fluorescence intensity. In addition to using the Raman transition with $F = 1, m_F = 0$–$F = 2, m'_F = 0$, which is insensitive to the first-order Zeeman shift, we also placed a two-layered magnetic shield over the interferometer section to further suppress the second-order Zeeman shift. The vacuum chamber and magnetic shields enclosing the interferometers, along with optical components, were constructed on a three-axis rotation optical table (custom-made by SIGMAKOKI Co., Ltd.). For the yaw axis, rotation in the range of ±15° at angular velocities up to 1 °/s is available. For the other axes, tilting is provided in the range ±4°.

Figure 3 shows the angular velocity dependence of the contrast of interference for right- and left-oriented atomic beams. The value was normalized to the contrast without rotation of the optical table. The contrast dependence on the angular velocity with the open-loop measurement was in good agreement with the theoretical prediction calculated using Eq. (2). In the calculation, actual experimental conditions were used: the mean velocity of the atoms at 100 °C escaping from the tube was $v \sim 330$ m/s, and the arm length was 70 mm. The shifts in the peak positions in the theoretical curve for the open-loop measurement were due to the phase shift caused by the two-photon detuning of the second Raman beam ($\Delta\omega_2$) for lock-in detection. The contrast was maximized at the angular velocity where the actual rotation cancels out the phase shift. The slight deviation in the measured peak position from the theoretical curve in the interferometer with the left-oriented beam is attributed to the imperfect alignment of the relative angles of the Raman beams against the atomic beam. For closed-loop dispersion compensation, the two-photon detunings for the first and third Raman beams ($\Delta\omega_1$ and $\Delta\omega_3$) were adjusted such that the closed-loop condition described in Eq. (7) was achieved. We confirmed that the contrast of the atom interferometers was maintained with the closed-loop method at an angular velocity of 0.6 °/s, whereas the contrast deteriorated to 1/5 with the open-loop measurement. We also validated that the contrast did not decay up to an angular velocity of 1 °/s, which was limited by the performance of the table.

To evaluate the stability of the scale factor, we simultaneously measured the angular velocity of the table using the AIG and a commercial FOG (Exail, blueSeis-3A). The scale-factor stability of the FOG was below 300 ppm, providing sufficient reliability for validating the concept of our closed-loop technique. Figure 4(a) shows the angular velocity measured using the AIG with open- and closed-loop measurements as a function of the value evaluated using the FOG. The angular velocity was calculated using Eqs. (6) and (7) for the open- and closed-loop measurements, respectively. Figure 4(b) shows the residual of the linear fitting of the measured data. Nonlinearity of the scale factor was observed in the open-loop measurements. This could be because the higher-order term was neglected in the discussion in the previous sections [31,47]. The error bars increased with increasing angular velocity, indicating that interferometer contrast decreased due to dephasing induced by rotation. In the closed-loop measurements, the linearity of the AIG was maintained at an angular

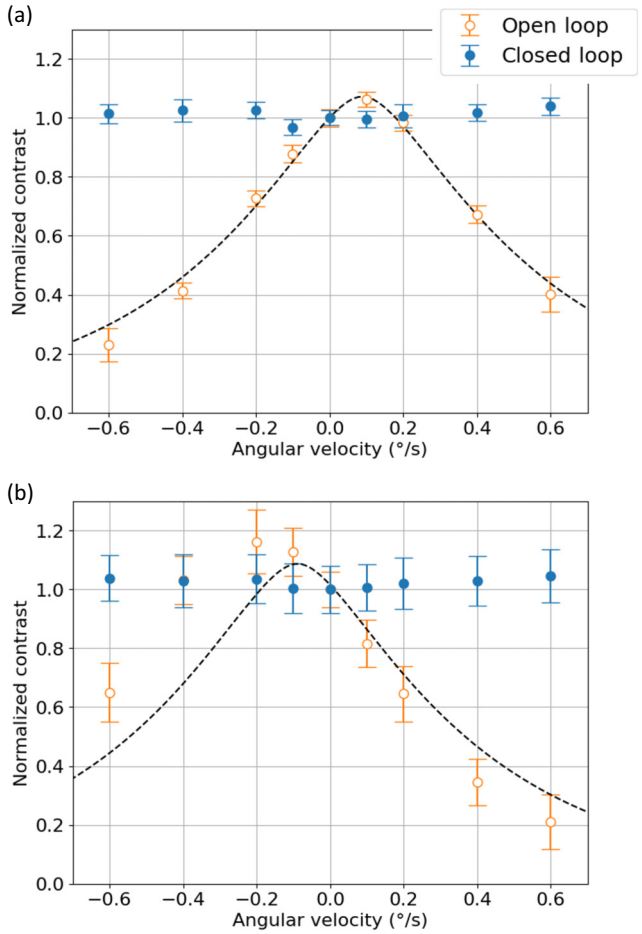

FIG. 3. Angular velocity dependence of the contrast of the interferometer with (a) right- and (b) left-oriented atomic beams. The values are normalized by the contrast without rotation. The dashed lines represent the theoretical estimations without the closed-loop rotation compensation for the actual experimental condition. Open and filled circles represent the experimental values for open- and closed-loop measurements, respectively.

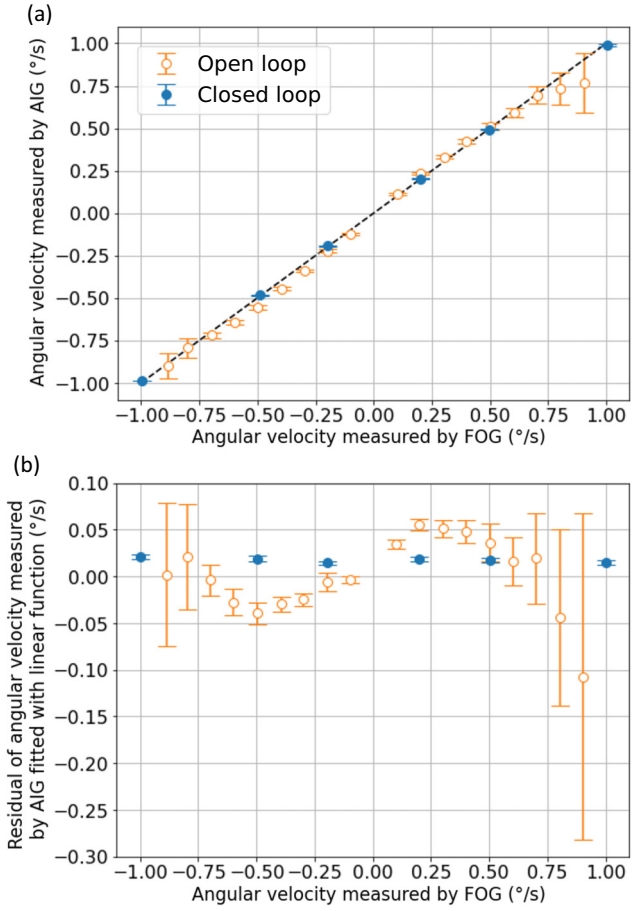

FIG. 4. (a) Comparison of the angular velocities measured by the AIG and the FOG. The dashed line represents the fitting result with a linear function for closed-loop measurements. (b) Residual errors in the linear fitting of the values obtained from open- and closed-loop measurements. In both plots, open and filled circles represent the experimental values for open- and closed-loop measurements, respectively.

velocity of 1 °/s. Because the contrast of the interference did not decrease, the error bars remained small even at high angular velocity. The slope of the linear fitting of the data acquired using the closed-loop control was 0.9901. The scale-factor error was 9900 ppm, significantly larger than the FOG's 300 ppm. The cause of this error could be a misalignment in the Raman light separation or another systematic error source, which will be addressed in Sec. IV.

The acceleration degrades interference contrast, whereas it does not cause a systematic error for measurement of rotational phase shift. We confirmed this feature by evaluating the angular velocity of the system while applying constant acceleration using a projective component of Earth's gravity in the closed-loop measurements, as shown in Fig. 5. In the first measurement, the rotation table was leveled horizontally. For the second and third measurements, acceleration was applied to the axis to which the interferometer was sensitive. When the optical table was tilted by 4° along this axis, this resulted in an acceleration of 0.68 m/s^2. Consequently, a phase offset of 28.4° was observed for both interferometers. Even if the phases of individual interferometers changed due to acceleration, the difference between them was not affected, allowing for accurate angular velocity measurements. In the fourth and fifth measurements, the interferometer was not sensitive to acceleration, whereas the velocity of the atom was affected, causing an error in the scale factor in the open-loop measurements. For the closed-loop measurements, because the scale factor did not include the velocity of the atoms, the measured values were unaffected.

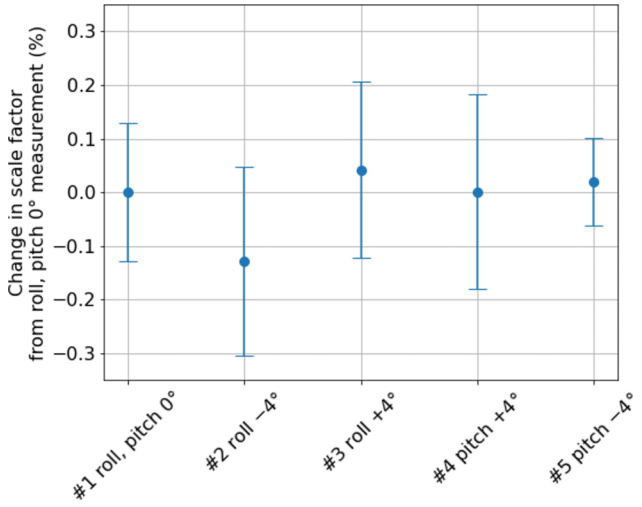

FIG. 5. Scale-factor changes in the rotation measurements with pitch and roll rotation of the table in the closed-loop measurements. Run #1: measurement taken with the rotation table horizontal. Runs #2 and #3: measurements taken with the table tilted by $\pm 4^{\circ}$ along the axis in the direction of the atomic beam. Runs #4 and #5: measurements taken with the table tilted by $\pm 4^{\circ}$ along the direction of the Raman beam axis. Measured changes in the scale factor are normalized by the value in Run #1.

IV. DISCUSSION

In Sec. II, we assumed an ideal setup for the atomic-beam gyroscope to illustrate the core concept of the closed-loop angular velocity measurement. In this section, we address several systematic errors arising from imperfections in the experimental setup.

The distance between the last Raman beam and the detection region, L_{det}, can differ for the right- and left-oriented atomic beams. By substituting L_{det} into Eqs. (4a) and (4b) with $L_{\mathrm{det,R}}$ and $L_{\mathrm{det,L}}$, Eq. (5) is modified as follows:

$$\Delta\Phi(\Omega) = 4k_{\mathrm{eff}}\Omega\frac{L^2}{v} - [2L(\Delta\omega_1 - \Delta\omega_3) + (L_{\mathrm{det,R}} - L_{\mathrm{det,L}})(\Delta\omega_1 - 2\Delta\omega_2 + \Delta\omega_3)]\frac{1}{v} = 0. \tag{8}$$

Assuming that the two-photon detuning of the first and third Raman beams is $\Delta\omega_1 = -\Delta\omega_3 = \Delta\omega$, the angular velocity can be deduced as

$$\Omega = \frac{\Delta\omega}{k_{\mathrm{eff}}L} - \frac{(L_{\mathrm{det,R}} - L_{\mathrm{det,L}})\Delta\omega_2}{2k_{\mathrm{eff}}L^2} \tag{9}$$

in the closed-loop measurements. For the lock-in detection of angular velocity Ω, $\Delta\omega_2$ must be set to a nonzero value, which introduces a systematic error into the measurement [the second term in Eq. (9)]; however, this systematic error can be compensated with a single initial calibration of the measured angular velocity, provided $\Delta\omega_2$ remains unchanged. Note that $|L_{\mathrm{det,R}} - L_{\mathrm{det,L}}|$ can be minimized by adjusting the position of the probe light so that the measured angular velocity becomes independent of changes in $\Delta\omega_2$ under a constant angular velocity.

Next, we discuss the systematic error caused by the mismatch in the velocity distribution of counterpropagating atomic beams. For simplicity, we assume that the counterpropagating atomic beams have monochromatic velocities of $v_{\mathrm{R}} = v, v_{\mathrm{L}} = -\alpha v$, where α is a positive constant. Accordingly, Eq. (5) should be modified as follows:

$$\Delta\Phi(\Omega, a) = 2k_{\mathrm{eff}}\Omega\frac{L^2}{v}\frac{\alpha+1}{\alpha} + k_{\mathrm{eff}}a\frac{L^2}{v^2}\frac{\alpha^2-1}{\alpha^2} - 2\Delta\omega\frac{L}{v}\frac{\alpha+1}{\alpha} + 2\Delta\omega_2\frac{L+L_{\mathrm{det}}}{v}\frac{\alpha-1}{\alpha} = 0, \tag{10}$$

with $\Delta\omega_1 = -\Delta\omega_3 = \Delta\omega$. From Eq. (10), Ω can be derived as

$$\Omega = \frac{\Delta\omega}{k_{\mathrm{eff}}L} + \frac{\alpha-1}{\alpha}\frac{a}{2v} + \frac{\alpha-1}{\alpha+1}\frac{L+L_{\mathrm{det}}}{k_{\mathrm{eff}}L^2}\Delta\omega_2. \tag{11}$$

When a and $\Delta\omega_2$ have finite values, the estimated value of Ω will depend on the difference in the velocities of the counterpropagating atomic beams. Here, we evaluate the systematic error in angular velocity measurement that arises when a slight temperature difference occurs between the left and right atomic ovens. In the following simulation, we used Eq. (2) instead of Eq. (11), as it accounts for the velocity distribution of each atomic beam. We employed an AIG using ^{87}Rb atomic beams with an arm length L of 70 mm. Further, $L_{\mathrm{det,R}}$ and $L_{\mathrm{det,L}}$ were set to the same length (125 mm) because these values could be precisely adjusted using the method stated previously. The temperatures of the atomic sources were set at 100 °C and 101 °C, assuming an upper limit for the temperature difference that would be achievable with a commercial temperature controller. The velocity distributions of the atoms were obtained using the Boltzmann distribution of the free molecular flow escaping from the tube channel [48]. Under the condition of $\Delta\omega_2/2\pi = 100$ Hz adopted in the current experiment, a phase shift corresponding to 5×10^{-5} °/s (9×10^{-7} rad/s) was induced. Using the recently proposed method of signal acquisition through phase modulation without frequency sweeping of the Raman light [49], the systematic error due to finite $\Delta\omega_2$ can be eliminated because $\Delta\omega_2$ can be set to zero. With a finite acceleration of $a = 0.68$ m/s^2, which was applied in this experiment, a phase shift corresponding to 7×10^{-5} °/s (1×10^{-6} rad/s) appears. This systematic error can be eliminated through a real-time correction using Kalman filtering with acceleration of the system and temperature of sources measured by other sensors.

Finally, we discuss the maximum angular velocity measurable with our closed-loop method. As long as the Sagnac phase depends solely on $1/v$, our closed-loop technique can be applied to atomic beams with any velocity distribution, effectively preventing a reduction in interferometer contrast; however, deviations from this analysis are expected at high angular velocities, where higher-order terms such as $1/v^2$ become significant. We numerically simulated the system response under the high angular velocity, and we found that the interference contrast is reduced to $1/e$ at an angular velocity of 3×10^3 °/s for our experimental parameters. This is because the trajectories of the atoms are bent by the Coriolis force, causing the time of flight between the first and second Raman beams to differ from that between the second and third Raman beams.

In the discussion of this paper, we used the simplification that the direction of the atomic beams, the direction of the Raman light propagation and acceleration, and the angular velocity are mutually orthogonal. When this relationship is not satisfied, cross-couplings due to higher-order contributions will affect the rotational measurements. Most of the higher-order terms cannot be canceled using our current method. In addition, cross-coupling due to three-dimensional motion will limit the dynamic range of the measurements [33]. A more detailed evaluation of these effects with theoretical and experimental aspects will be presented in forthcoming papers.

V. SUMMARY

The Sagnac phase, which reflects the rotation in atom interferometry, depends on the velocity of the atoms. Due to the longitudinal velocity distribution of the atoms, individual atoms within the interferometer produce varying interference phases, and this results in reduced signal amplitude due to phase dispersion. We introduce a method to restore the contrast degradation in an AIG. By adjusting the frequency detunings of the Raman light beams that construct the atom interferometer, we can induce a velocity-dependent phase shift similar to that of the Sagnac effect. This introduces a pseudorotation effect that can cancel the rotation of all atoms, even those with a broad distribution of longitudinal velocities. Applying this method to an AIG with counterpropagating atomic beams sharing the same Raman light, we also observed that the angular velocity of the system can be determined independently of the velocity of the atoms from the two-photon detunings at which the phase difference between the two interferometers becomes zero. We validated our method using an AIG with thermal atomic beams of ^{87}Rb and closed-loop rotation measurements on a three-axis rotation table. The contrast of the interference was maintained even at an angular velocity of 0.6 °/s, which was a significant improvement compared to the 1/5 contrast decrease observed without compensation. The angular velocities measured using the closed-loop AIG were linearly proportional to those measured using the commercial FOG up to an angular velocity of 1.0 °/s. We also demonstrated the robustness of our closed-loop angular velocity measurements against acceleration, using the projective component of gravity within the table's roll and pitch tilting in the range of ±4°. We performed numerical calculations and found that potential systematic errors can be eliminated by combining our method with other techniques and measurements. With its simple and robust closed-loop mechanism using two-photon detuning of Raman light, our method holds promise for high-dynamic-range applications such as the inertial navigation of vehicles.

ACKNOWLEDGMENTS

We thank Ryotaro Inoue and Yuichiro Kamino for helpful discussions. This work was supported by the Japan Science and Technology Agency (JST), Grants No. JPMJMI17A3 and JPMJPF2015.

[1] M. Kasevich and S. Chu, Atomic interferometry using stimulated Raman transitions, Phys. Rev. Lett. **67**, 181 (1991).
[2] M. Kasevich and S. Chu, Measurement of the gravitational acceleration of an atom with a light-pulse atom interferometer, Appl. Phys. B **54**, 321 (1992).
[3] J. Lautier, L. Volodimer, T. Hardin, S. Merlet, M. Lours, F. Pereira Dos Santos, and A. Landragin, Hybridizing matter-wave and classical accelerometers, Appl. Phys. Lett. **105**, 144102 (2014).
[4] P. Cheiney, L. Fouch, S. Templier, F. Napolitano, B. Battelier, P. Bouyer, and B. Barrett, Navigation-compatible hybrid quantum accelerometer using a Kalman filter, Phys. Rev. Appl. **10**, 034030 (2018).
[5] T. L. Gustavson, A. Landragin, and M. A. Kasevich, Rotation sensing with a dual atom-interferometer Sagnac gyroscope, Classical Quantum Gravity **17**, 2385 (2000).
[6] D. S. Durfee, Y. K. Shaham, and M. A. Kasevich, Long-term stability of an area-reversible atom-interferometer Sagnac gyroscope, Phys. Rev. Lett. **97**, 240801 (2006).
[7] D. Savoie, M. Altorio, B. Fang, L. A. Sidorenkov, R. Geiger, and A. Landragin, Interleaved atom interferometry for high-sensitivity inertial measurements, Sci. Adv. **4**, eaau7948 (2018).
[8] C. Avinadav, D. Yankelev, M. Shuker, O. Firstenberg, and N. Davidson, Rotation sensing with improved stability using point-source atom interferometry, Phys. Rev. A **102**, 013326 (2020).
[9] M. Gebbe, J.-N. Siem, M. Gersemann, H. Mntinga, S. Hermann, C. Lmmerzahl, H. Ahlers, N. Gaaloul, C. Schubert, K. Hammerer, S. Abend, and E. M. Rasel, Twin-lattice atom interferometry, Nat. Commun. **12**, 2544 (2021).
[10] A. Peters, K. Y. Chung, and S. Chu, High-precision gravity measurements using atom interferometry, Metrologia **38**, 25 (2001).

[11] Z.-K. Hu, B.-L. Sun, X.-C. Duan, M.-K. Zhou, L.-L. Chen, S. Zhan, Q.-Z. Zhang, and J. Luo, Demonstration of an ultrahigh-sensitivity atom-interferometry absolute gravimeter, Phys. Rev. A **88**, 043610 (2013).

[12] C.-Y. Li, J.-B. Long, M.-Q. Huang, B. Chen, Y.-M. Yang, X. Jiang, C.-F. Xiang, Z.-L. Ma, D.-Q. He, L.-K. Chen, and S. Chen, Continuous gravity measurement with a portable atom gravimeter, Phys. Rev. A **108**, 032811 (2023).

[13] M. J. Snadden, J. M. McGuirk, P. Bouyer, K. G. Haritos, and M. A. Kasevich, Measurement of the Earth's gravity gradient with an atom interferometer-based gravity gradiometer, Phys. Rev. Lett. **81**, 971 (1998).

[14] J. M. McGuirk, G. T. Foster, J. B. Fixler, M. J. Snadden, and M. A. Kasevich, Sensitive absolute-gravity gradiometry using atom interferometry, Phys. Rev. A **65**, 033608 (2002).

[15] G. Rosi, F. Sorrentino, L. Cacciapuoti, M. Prevedelli, and G. M. Tino, Precision measurement of the Newtonian gravitational constant using cold atoms, Nature **510**, 518 (2014).

[16] R. H. Parker, C. Yu, W. Zhong, B. Estey, and H. Müller, Measurement of the fine-structure constant as a test of the Standard Model, Science **360**, 191 (2018).

[17] S. Dimopoulos, P. W. Graham, J. M. Hogan, M. A. Kasevich, and S. Rajendran, Atomic gravitational wave interferometric sensor, Phys. Rev. D **78**, 122002 (2008).

[18] B. Canuel, *et al.*, Exploring gravity with the MIGA large scale atom interferometer, Sci. Rep. **8**, 14064 (2018).

[19] M.-S. Zhan, *et al.*, ZAIGA: Zhaoshan long-baseline atom interferometer gravitation antenna, Int. J. Mod. Phys. D **29**, 1940005 (2020).

[20] M. Abe, *et al.*, Matter-wave Atomic Gradiometer Interferometric Sensor (MAGIS-100), Quantum Sci. Technol. **6**, 044003 (2021).

[21] C. D. Panda, M. J. Tao, M. Ceja, J. Khoury, G. M. Tino, and H. Mller, Measuring gravitational attraction with a lattice atom interferometer, Nature **631**, 515 (2024).

[22] R. Geiger, V. Ménoret, G. Stern, N. Zahzam, P. Cheinet, B. Battelier, A. Villing, F. Moron, M. Lours, Y. Bidel, A. Bresson, A. Landragin, and P. Bouyer, Detecting inertial effects with airborne matter-wave interferometry, Nat. Commun. **2**, 474 (2011).

[23] B. Barrett, L. Antoni-Micollier, L. Chichet, B. Battelier, T. Lévèque, A. Landragin, and P. Bouyer, Dual matter-wave inertial sensors in weightlessness, Nat. Commun. **7**, 13786 (2016).

[24] Y. Bidel, N. Zahzam, C. Blanchard, A. Bonnin, M. Cadoret, A. Bresson, D. Rouxel, and M. F. Lequentrec-Lalancette, Absolute marine gravimetry with matter-wave interferometry, Nat. Commun. **9**, 627 (2018).

[25] Y. Bidel, N. Zahzam, A. Bresson, C. Blanchard, M. Cadoret, A. V. Olesen, and R. Forsberg, Absolute airborne gravimetry with a cold atom sensor, J. Geod. **94**, 20 (2020).

[26] L. Antoni-Micollier, M. Arnal, R. Gautier, C. Janvier, V. Ménoret, J. Richard, P. Vermeulen, P. Rosenbusch, C. Majek, and B. Desruelle, Absolute quantum gravimeters and gradiometers for field measurements, IEEE Instrum. Meas. Mag. **27**, 4 (2024).

[27] D. Titterton and J. L. Weston, *Strapdown Inertial Navigation Technology* (Institution of Engineering and Technology, London, 2004), 2nd ed.

[28] H. C. Lèfevre, *et al.*, in *Optical Waveguide and Laser Sensors* (SPIE, 2020), Vol. 11405, p. 10, https://www.spiedigitallibrary.org/conference-proceedings-of-spie/11405/1140505/The-fiber-optic-gyro-adventure-at-Photonetics-iXsea-and-now/10.1117/12.2560791.full?webSyncID=50a4ae28-7100-3dce-ba8a-aa283e8c0734&sessionGUID=9c260d3d-0b67-b79a-e1de-3715ea37b20d.

[29] H. C. Lèfevre, *The Fiber-Optic Gyroscope* (Artech House, Boston, 2022), 3rd ed.

[30] N. Song, X. Xu, Z. Zhang, F. Gao, and X. Wang, Advanced interferometric fiber optic gyroscope for inertial sensing: A review, J. Lightwave Technol. **41**, 4023 (2023).

[31] J. M. Hogan, D. M. S. Johnson, and M. A. Kasevich, in *Atom Optics and Space Physics* (IOS Press, Amsterdam, 2009), p. 411.

[32] J. Fang and J. Qin, Advances in atomic gyroscopes: A view from inertial navigation applications, Sensors **12**, 6331 (2012).

[33] F. A. Narducci, A. T. Black, and J. H. Burke, Advances toward fieldable atom interferometers, Adv. Phys.: X **7**, 1946426 (2022).

[34] G. Sagnac, L'ether lumineux demontre par l'effet du vent relatif d'ether dans un interferometre en rotation uniforme, C. R. Acad. Sci. **157**, 708 (1913).

[35] G. Sagnac, Sur la preuve de la ralit de l'éfther lumineux par l'expérience de l'interférographe tournant, C. R. Acad. Sci. **157**, 1410 (1913).

[36] P. Storey and C. Cohen-Tannoudji, The Feynman path integral approach to atomic interferometry. A tutorial, J. Phys. II **4**, 1999 (1994).

[37] J. Kwolek, C. Fancher, M. Bashkansky, and A. Black, Three-dimensional cooling of an atom-beam source for high-contrast atom interferometry, Phys. Rev. Appl. **13**, 044057 (2020).

[38] Q. d'Armagnac de Castanet, C. Des Cognets, R. Arguel, S. Templier, V. Jarlaud, V. Mnoret, B. Desruelle, P. Bouyer, and B. Battelier, Atom interferometry at arbitrary orientations and rotation rates, Nat. Commun. **15**, 6406 (2024).

[39] C. R. Ekstrom, J. Schmiedmayer, M. S. Chapman, T. D. Hammond, and D. E. Pritchard, Measurement of the electric polarizability of sodium with an atom interferometer, Phys. Rev. A **51**, 3883 (1995).

[40] M. Jacquey, A. Miffre, G. Trénec, M. Büchner, J. Vigué, and A. Cronin, Dispersion compensation in atom interferometry by a Sagnac phase, Phys. Rev. A **78**, 013638 (2008).

[41] A. Roura, Circumventing Heisenberg's uncertainty principle in atom interferometry tests of the equivalence principle, Phys. Rev. Lett. **118**, 160401 (2017).

[42] P. Asenbaum, C. Overstreet, M. Kim, J. Curti, and M. A. Kasevich, Atom-interferometric test of the equivalence principle at the 10^{-12} level, Phys. Rev. Lett. **125**, 191101 (2020).

[43] H. Ahlers, *et al.*, STE-QUEST: Space Time Explorer and QUantum Equivalence principle Space Test, ArXiv:2211.15412v3.

[44] P. R. Berman, ed.*Atom Interferometry* (Academic Press, San Diego, 1997), 1st ed.

[45] Y. Luo, J. You, Q. Hu, Y. Li, M. Ma, J. Wang, and F. Xu, Reanalyzing atomic beam interferometric gyroscopes: Dependence of sensitivity on experimental parameters, IEEE Sens. J. **21**, 1433 (2021).

[46] A. Joyet, G. Di Domenico, and P. Thomann, Theoretical analysis of aliasing noises in cold atom Mach-Zehnder interferometers, Eur. Phys. J. D **66**, 61 (2012).

[47] K. Bongs, R. Launay, and M. Kasevich, High-order inertial phase shifts for time-domain atom interferometers, Appl. Phys. B **84**, 599 (2006).

[48] N. Ramsey, *Molecular Beams* (Oxford University Press, Oxford, 1986).

[49] T. Kawasaki, S. Otabe, T. Sato, M. Miranda, N. Takei, and M. Kozuma, Analyzing the sensitivity of an atom interferometer with a phase modulation readout scheme, Phys. Rev. A **111**, 013302 (2025).